Biosensors and Bioelectronics 77 (2016) 471–477

Contents lists available at ScienceDirect

Biosensors and Bioelectronics

journal homepage: www.elsevier.com/locate/bios

In vivo sensing of proteolytic activity with an NSET-based NIR fluorogenic nanosensor

Minhee Ku [a,b,1], Yoochan Hong [a,c,1], Dan Heo [a,d], Eugene Lee [a,d], Seungyeon Hwang [a], Jin-Suck Suh [a,b,c,d], Jaemoon Yang [a,b,c,*]

[a] Department of Radiology, College of Medicine, Yonsei University, Seoul 03722, Republic of Korea
[b] Brain Korea 21 Plus Project for Medical Science, Yonsei University, Seoul 03722, Republic of Korea
[c] YUHS-KRIBB Medical Convergence Research Institute, Seoul 03722, Republic of Korea
[d] Nanomedical National Core Research Center, Yonsei University, Seoul 03722, Republic of Korea

ARTICLE INFO

Article history:
Received 3 September 2015
Received in revised form
27 September 2015
Accepted 28 September 2015
Available online 30 September 2015

Keywords:
Nanoparticle surface energy transfer
Gold nanorod
Fluorogenic
Membrane type 1-matrix metalloproteinase
Nanosensor

ABSTRACT

Biomedical *in vivo* sensing methods in the near-infrared (NIR) range, which that provide relatively high photon transparency, separation from auto-fluorescence background, and extended sensitivity, are being used increasingly for non-invasive mapping and monitoring of molecular events in cancer cells. In this study, we fabricated an NIR fluorogenic nanosensor based on the nanoparticle surface energy transfer effect, by conjugation of fluorescent proteolytic enzyme-specific cleavable peptides with gold nanorods (GNRs). Membrane-anchored membrane type 1-matrix metalloproteinases (MT1-MMPs), a family of zinc-dependent proteolytic enzymes, can induce the metastatic potential of cancer cells by promoting degradation of the extracellular matrix. Therefore, sensitive detection of MT1-MMP activity can provide essential information in the clinical setting. We have applied *in vivo* NIR sensing to evaluate MT1-MMP activity, as an NIR imaging target, in an MT1-MMP-expressing metastatic tumor mouse model.

1. Introduction

Optical bio-sensing techniques using bioluminescence and fluorescence lights are an attractive sensing modality for non-invasively visualization of disease progress at the molecular level and provide meaningful preclinical and clinical information (Cheng et al. 2006; Ke et al. 2003). However, in these sensing modalities, most of the light does not penetrate relatively deep into soft tissues. Moreover, interference from other tissue pigments further limits the clinical and research applications of optical sensing. To overcome these limitations to its use, many researchers have developed fluorescent probes that exhibit biological stability and specific accumulation at the target site and function in the "tissue optical window" (Quek and Leong 2012; Tsai et al. 2001). The near-infrared (NIR) spectral radiation (about 700–1000 nm in wavelength) can be transmitted several centimeters into biological tissues and causes less thermal damage or other light-tissue interaction than the light in other bio-sensing methods and thus, NIR sensing offers a potentially dynamic non-invasive sensing method for assessing biological events in an *in vivo* environment (Ke et al. 2003; Tsai et al. 2001). In particular, cyanine (Cy) dyes have been widely used as sensing agents for tumor-bearing animals because of their strong tissue penetration ability. Particularly, Cy7 is suitable for labeling biological molecules located in large tissue masses due to its long excitation and emission wavelengths (747/776 nm), compared with other Cy fluorochromes (Ballou et al. 1998; Zou et al. 2009).

The potential applications of nanoparticles has attracted considerable interest in their use in molecular sensing, as well as for providing targeted treatment options and improving techniques in cancer diagnosis (Smith et al. 2012). In particular, gold nanorods (GNRs) have been used as specific carriers of various agents against cancer for *in vivo* and *in vitro* research (Bonoiu et al. 2011; Masood et al. 2012; Xiao et al. 2012). GNRs have many potential biomedical applications, including sensing, photothermal therapy, and drug delivery; in addition, GNRs are also effectively fluorescence-quenched when fluorescent molecules are located in their vicinity (Tiwari et al. 2011; Zhang et al. 2013). This quenching effect, based on nanoparticle surface energy transfer (NSET), provides an outstanding low signal-to-noise ratio and allows for simultaneous multiple fluorescence quenching effects at differing energies. GNRs have two different localized surface plasmon resonance bands, the transverse band and the longitudinal band, depending on its axis (Law et al. 2009; Peng and Pachpinde 2014). The longitudinal band presents more sensitive scattering and

* Corresponding author at: Department of Radiology, College of Medicine, Yonsei University, Seoul 03722, Republic of Korea.
E-mail address: 177hum@yuhs.ac (J. Yang).
[1] These authors equally contributed to this work.

http://dx.doi.org/10.1016/j.bios.2015.09.067
0956-5663/

absorption (Law et al. 2009). Therefore, there are optical advantages in using GNRs, including the enhancement of the quenching efficiency that is related to the spectral overlap of GNR absorption and the emission spectra of other chromophores, enabling the NSET effect (Ghosh and Chattopadyay 2013).

The enzymatic activity of proteinases is an important biological feature that is associated with cancer metastasis (Gialeli et al. 2011). Especially, recent studies have suggested the pivotal role played by membrane type 1-matrix metalloproteinase (MT1-MMP) in promoting the malignant behavior of cancer cells, including rapid tumor growth, invasion, and metastasis *via* degradation of the extracellular matrix (Kessenbrock et al. 2010; Seiki 2003; Zhai et al. 2005). Moreover, metastatic cancer cells that express MT1-MMP exhibit increased glycolytic activity, and forced expression of MT1-MMP in MT1-MMP-negative cancers is sufficient to induce the Warburg effect (Andersson et al. 2007). For these reasons, methods for sensing MT1-MMP activity as well as detection of specific biomarker expression in cancer would be invaluable tools in cancer diagnosis and treatment.

We have recently identified a protease-specific activatable fluorogenic peptide (ActFP) sequence suitable for a non-invasive molecular sensing nanoprobe for detection of MT1-MMP by protease-mediated endocytosis (Lee et al. 2012; Park et al. 2012). In a previous study, we prepared fluorogenic nanoprobes using a combination of gold nanoparticles, with a maximum characteristic peak at about 520 nm, and fluorescein isothiocyanate (Hong et al. 2014). However, the fluorogenic nanoprobes in that study were operative in the visible region, making them unsuitable for *in vivo* studies.

In this report, we describe an NSET-based fluorogenic nanosensor using an MT1-MMP-specific cleavable peptide (MSCP) labeled with the NIR fluorescence dye (Cy7) and GNRs. This fluorogenic nanosensor was developed for non-invasive *in vivo* sensing of MT1-MMP activity for metastatic tumors in a xenograft mouse model (Scheme 1). ActFP was synthesized based on MSCP, conjugated with Cy7 and then immobilized onto GNRs for efficient induction of the NSET effect and generation of active fluorogenic signal by MT1-MMP. The optimal conditions, i.e., the ActFP concentration, for NSET and fluorogenic effects from GNR-ActFP were determined. Furthermore, *in vitro* and *in vivo* targeted sensing studies were carried out using the newly-developed GNR-ActFP.

2. Materials and methods

2.1. Preparation of ActFP

Based on the previously reported MT1-MMP substrate, GPLPLRSWGLK (Hong et al. 2014), we designed a MT1-MMP-specific ActFP by conjugating the Cy7 fluorescence dye with the peptide. First, 0.81 mg of peptide (M_w: 1.504 Da) was dissolved into 1 mL of phosphate buffered saline (PBS), and 150 μL of Cy7 solution (1 mg/mL) was added to this reactant solution. Dopamine (1 mL; 0.1 mg/mL), 1-ethyl-3-(3-dimethylaminopropyl)-carbodiimide (0.41 mg), and sulfo-N-hydroxysulfosuccinimide (0.47 mg) were successively added to the solution, and the reaction mixture was incubated for 24 h. The resultant solution was dialyzed using a dialysis tube (MWCO: 1.000 Da) for 48 h and centrifuged using Centricon (MWCO: 3.000 Da) to remove impurities.

2.2. Preparation of GNR-ActFP

To prepare the monodisperse GNRs, a seed-mediated growth method was used, with some modifications (Hong et al. 2013). The GNRs were then chemically conjugated with polyethylene glycol (COOH-PEG-SH; M_w: 3.400 Da), and the concentration of GNRs was adjusted to 413 nM of Au after PEGylation. For preparation of GNR-ActFP, varying volumes of an ActFP stock solution (100 μM)

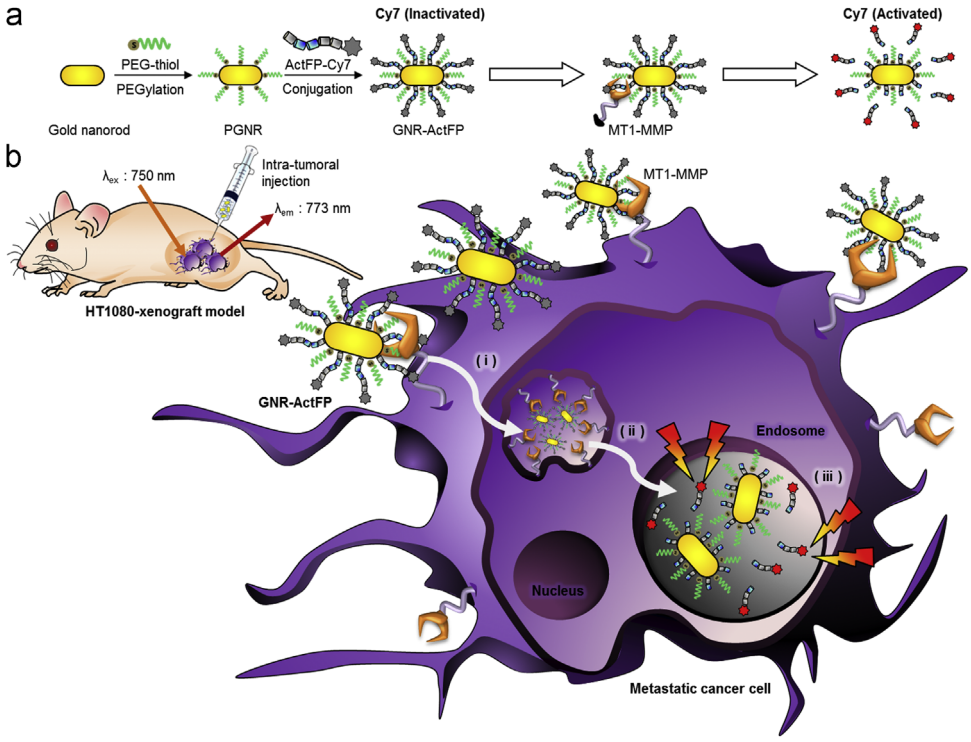

Scheme 1. Schematic illustration of the preparation of GNR-ActFP. (a) Synthetic procedures of Gold nanorod conjugated with MT1-MMP-sensitive activatable peptide (GNR-ActFP). (b) Schematic illustration of endocytosis mechanism of GNR-ActFP as a nanosensor for NIR sensing of MT1-MMP-expressing tumors in a mouse xenograft model; (i) MT1-MMP mediated endocytosis of GNR-ActFPs, (ii) peptide cleavage by proetolytic activity of MT1-MMP and (iii) GNR-ActFP activated and NIR fluorescence signal detected.

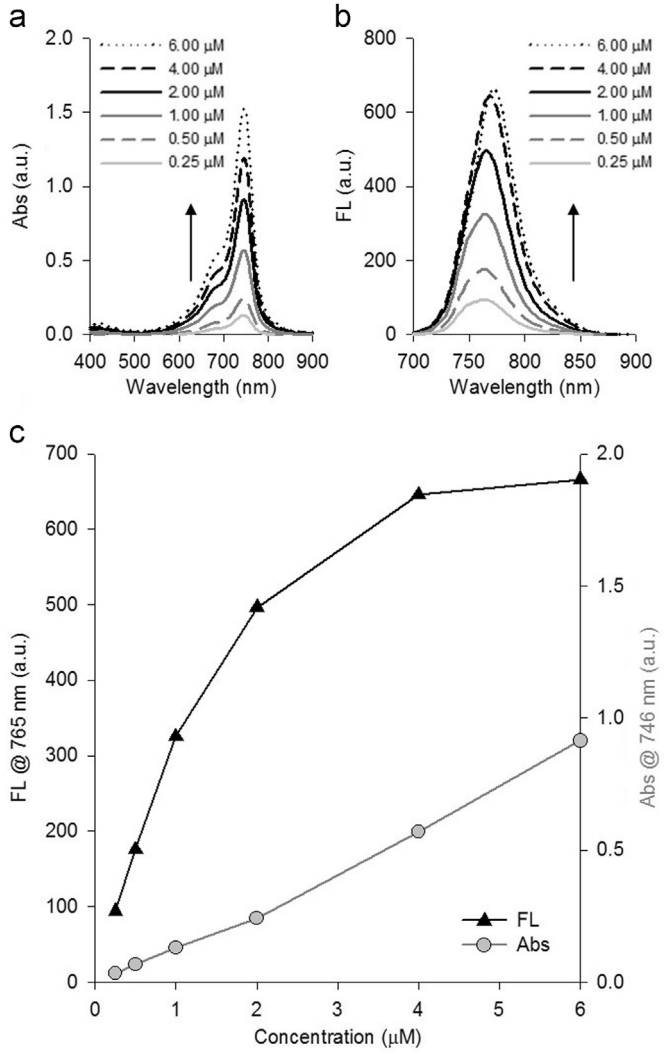

Fig. 1. Characterization of optical properties of ActFP. (a) Absorbance and (b) fluorescence spectra for ActFP at varying concentrations of ActFP. (c) Absorbance at 746 nm (gray circles) and fluorescence intensity at 765 nm (black triangles) for ActFP. Abs, absorbance; FL, fluorescence intensity; a.u., arbitrary units.

was added to the GNR solution. The final concentrations of ActFP in the GNR-ActFP were set to 6.00, 4.00, 2.00, 1.00, 0.50, and 0.25 μM, respectively. Additionally, the absorbance and fluorescence spectra of GNR, ActFP, and GNR-ActFP were determined using a spectrometer (Perkin Elmer, Lamda 25, USA) and spectrofluorometer (Jasco, FP-6500, Japan), respectively. The crystallinities for GNR and GNR-ActFP were analyzed using a high-resolution transmission electron microscope (HR-TEM, JEM-ARM 200F; JEOL Ltd., Tokyo, Japan). The chemical structure of ActFP and GNR-ActFP was analyzed using proton-nuclear magnetic resonance (^{1}H NMR; JUM-ECP300, JEOL Ltd., Japan) with deuterium oxide (D_2O) as the solvent.

2.3. Biocompatibility test

The cell viabilities for MT1-MMP-expressing HT1080 and MT1-MMP-deficient MCF7 cells treated with GNR-ActFP were evaluated using a colorimetric assay based on the mitochondrial oxidation of 3-(4, 5-dimethylthiazoly-2)-2, 5-diphenyltetrazolium bromide (MTT). In a typical cell viability experiment, HT1080 and MCF7 cells were seeded into 96-well plates (1×10^4 cells/well) and incubated at 37 °C in an atmosphere of 5% CO_2. The cells were incubated for 2 h with GNR-ActFP (the final concentrations of ActFP in the GNR-ActFP was 2 μM), and then the yellow MTT solution was treated. The formazan crystals formed were solubilized with 10% sodium dodecyl sulfate in 0.01 M HCl. Then, the absorbance of the resulting colored solution was measured at 584 nm, and at 650 nm as a reference wavelength, using a microplate spectrophotometer (Epoch™, BioTek, USA). Cell viability was calculated as the relative value, from the intensity ratio of treated to non-treated control cells. Data are represented as the mean ± standard deviation (SD; $n=4$).

2.4. In vitro fluorogenic study

HT1080 and MCF7 cells were seeded at 5×10^4 cells/well in 4-well plates and incubated at 37 °C in an atmosphere of 5% CO_2. These cells were treated with GNR-ActFP for 4 h at 37 °C and washed three times with PBS to eliminate free unbound GNR-ActFP. The uptake of GNR-ActFP was assessed using dark field images, captured with a high numerical aperture dark field condenser (Olympus, U-DCW, Japan), which delivers a very narrow beam of white light from a tungsten halogen lamp to the surface of the sample. Immersion oil (N.D.: 1.516) was used to narrow the gap between the condenser and the glass slide, and to balance the refractive index. The fluorescence of GNR-ActFP in cells was evaluated using a microplate spectrophotometer (Epoch™; BioTek, USA). For distinguishing the MT1-MMP activity, cells were seeded on 96-well Assay Black Plates with clear bottoms at a density of 1×10^4 cells/well and incubated overnight to allow cell attachment. Cells were plated in triplicate for each measurement and the data are represented as the mean ± SD. Plates were incubated at 37 °C in an atmosphere of 5% CO_2. The medium in the wells was replaced with the suspension of GNR-ActFPs and the fluorescence signal was measured immediately. To study the effect of incubation time on GNR-ActFP uptake, the plate was incubated for 0, 10, 20, and 30 min and the signal intensity was measured using a microplate spectrophotometer (Epoch™). The fluorescence signals were measured at $746_{ex}/765_{em}$. To estimate *in vitro* NIR sensing effect of GNR-ActFP, HT1080 and MCF7 cells were respectively seeded with 5×10^4 cells/well in 4-well plates and incubated overnight at 37 °C in an atmosphere of 5% CO_2. These cells were treated with PBS or GNR-ActFP for 4 h at 37 °C and then washed. NIR images of the HT1080 and MCF7 cells treated with GNR-ActFP were obtained using an IVIS® Imaging System (Xenogen, USA).

2.5. In vivo fluorogenic sensing

All animal experiments were conducted with the approval of the Association for Assessment and Accreditation of Laboratory Animal Care International. To establish orthotopic mouse model of fibrosarcoma, HT1080 cells (5×10^6 cells) were implanted into the proximal thigh of female mice. When the tumor size reached approximately 500 mm^3 (tumor volume in mm^3 was calculated using the following formula: tumor volume $= 4/3 \times \pi \times [\text{width}/2]^2 \times [\text{length}/2]^2$), GNR-ActFP was injected subcutaneously into the tumor site and normal opposite site. NIR images of the mouse model treated with GNR-ActFP were obtained with an IVIS® Imaging System.

3. Results and discussion

3.1. Characterization of Cy7-conjugated MSCP

For the manufacturing of efficient MT1-MMP-specific fluorogenic nanosensor, we determined the optimal concentration of the conjugated ActFP molecules against GNR. The optical properties of ActFP were analyzed at various ActFP concentrations (Fig. 1a and b).

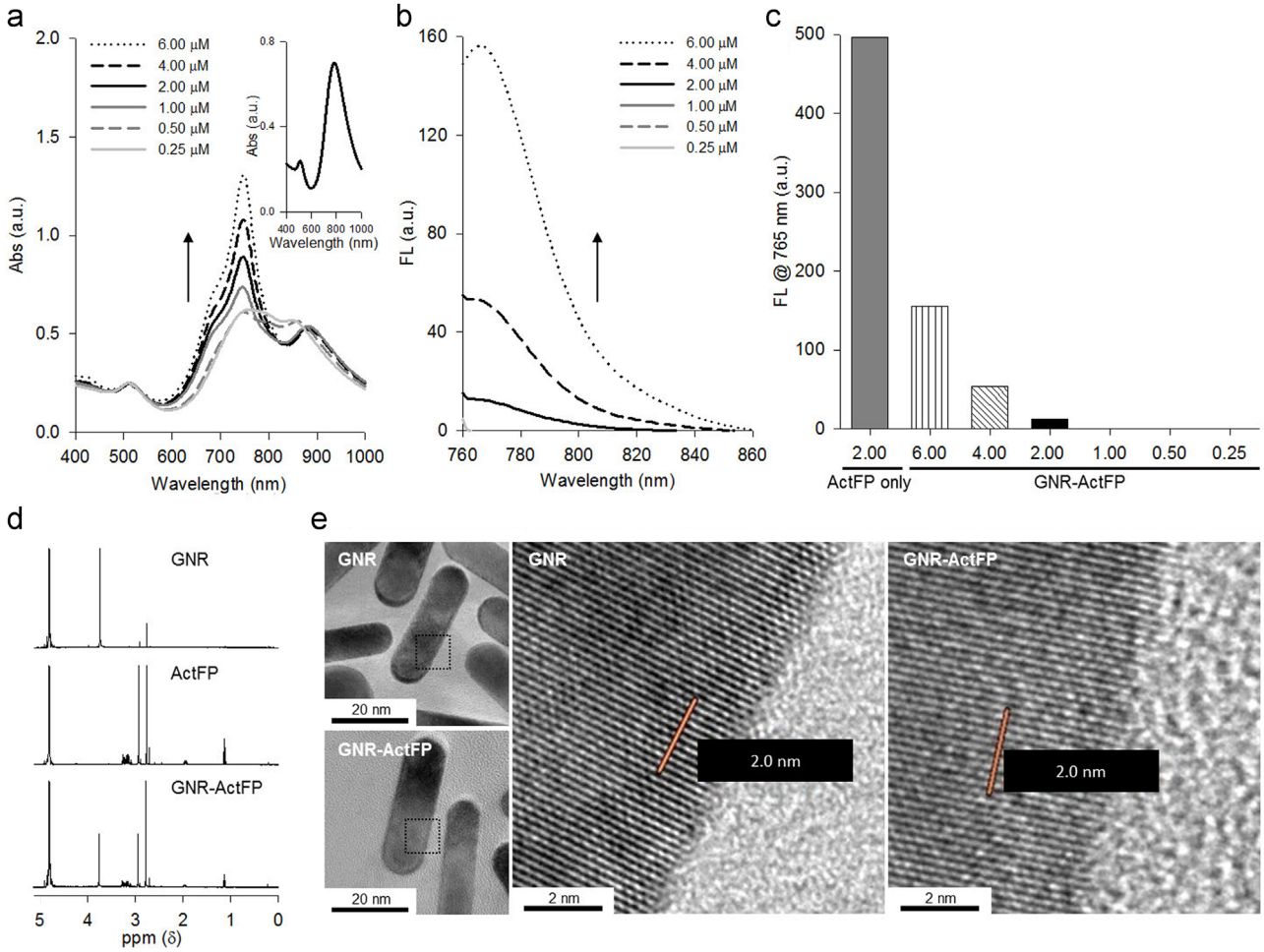

Fig. 2. Characterization of GNR-ActFP. (a) Absorbance and (b) florescence spectra for GNR-ActFP at varying concentrations of ActFP conjugated with GNR; inset in a: absorbance spectra for GNR. (c) Fluorescence intensity at 765 nm for 2 μM of ActFP only (the first bar) as shown in Fig. 1b, and for GNR-ActFP at varying concentrations of conjugated ActFP (the following bars). All subsequent experiments were conducted with 2 μM GNR-ActFP. (d) ^{1}H NMR spectra of GNR (upper), ActFP (middle), and GNR-ActFP (lower), respectively. (e) HR-TEM images for GNR (upper) and GNR-ActFP (lower). The enlarged individual HR-TEM images are inserted in lower column. Abs, absorbance; FL, fluorescence intensity; a.u., arbitrary units.

Because ActFP was composed of MSCP and Cy7, the absorbance and fluorescence spectra for ActFP were depend on the optical properties of Cy7. When the concentration of ActFP was increased, the absorbance at 746 nm, which corresponds to the characteristic peak for Cy7, was linearly raised (R^2=0.9976, Fig. 1c). However, the fluorescence intensity at the characteristic peak of Cy7 (765 nm) was saturated over 4.00 μM of ActFP due to the self-quenching effect at high concentrations (Andersson et al. 2007; Austin et al. 2005).

3.2. Characterization of fluorogenic nanosensor

To evaluate the efficiency of the NSET effect, moreover, the optical properties of GNR-ActFP were confirmed as a function of ActFP concentration. At low ActFP concentration, the absorbance at 746 nm was decreased (Fig. 2a), and the fluorescence intensity at 765 nm from GNR-ActFP was dramatically reduced (Fig. 2b). The fluorescence intensity at 785 nm for 2.00 μM of free ActFP was about 500 as shown in Fig. 1c. However, in the case of GNR-ActFP, the fluorescence intensity was approximately 40-fold lower than that of free ActFP, in spite of the presence of the same ActFP concentration (Fig. 2c). From these results, we could confirm the appropriate ActFP/GNR ratio for generating an effective MT1-MMP-specific fluorogenic nanosensor.

To verify the robustness of the prepared GNR-ActFP, the chemical structure of the conjugated ActFP and crystallinity of GNR were investigated. As shown in Fig. 2d, the characteristic peaks of ethylene glycol chain (–CH_2CH_2O–) were observed at 3.75 ppm in both PEGylated GNR and ActFP-GNR. The characteristic peaks of ActFP were observed at 1.12, 1.91, 2.77, and 2.93 ppm due to the hydrocarbon, hydrogen of amine group, and hydrogen of hydrocarbon. After the conjugation of ActFP with GNR, there was no critical shift compared to free ActFP. These results were coincidence with previously published reports (Choi et al. 2012, 2011). Furthermore, the crystallinities for GNR and GNR-ActFP were analyzed *via* HR-TEM (Fig. 2e). Both GNR and GNR-ActFP presented clear fringes and perfectly face-centered cubic single crystalline rods. Ten fringes spacing for both GNR and GNR-ActFP was 2.0, which corresponded well to the lattice spacing of the {200} planes for a single gold crystal (0.2 nm) (Si et al. 2012). Consequently, there are no significant differences in crystallinity between GNR and GNR-ActFP. These results indicate that ActFP was successfully conjugated with GNR for effective NSET-based nanosensor.

3.3. Determination of MT1-MMP-specific fluorogenic potential of GNR-ActFP in vitro

To evaluate MT1-MMP-specific NIR fluorogenic potentials of GNR-ActFP, cell viability was firstly confirmed after the treatment of GNR-ActFP against MT1-MMP-expressing HT1080 and MT1-MMP-deficient MCF7 cells. As shown in Fig. 3a, GNR-ActFP did not

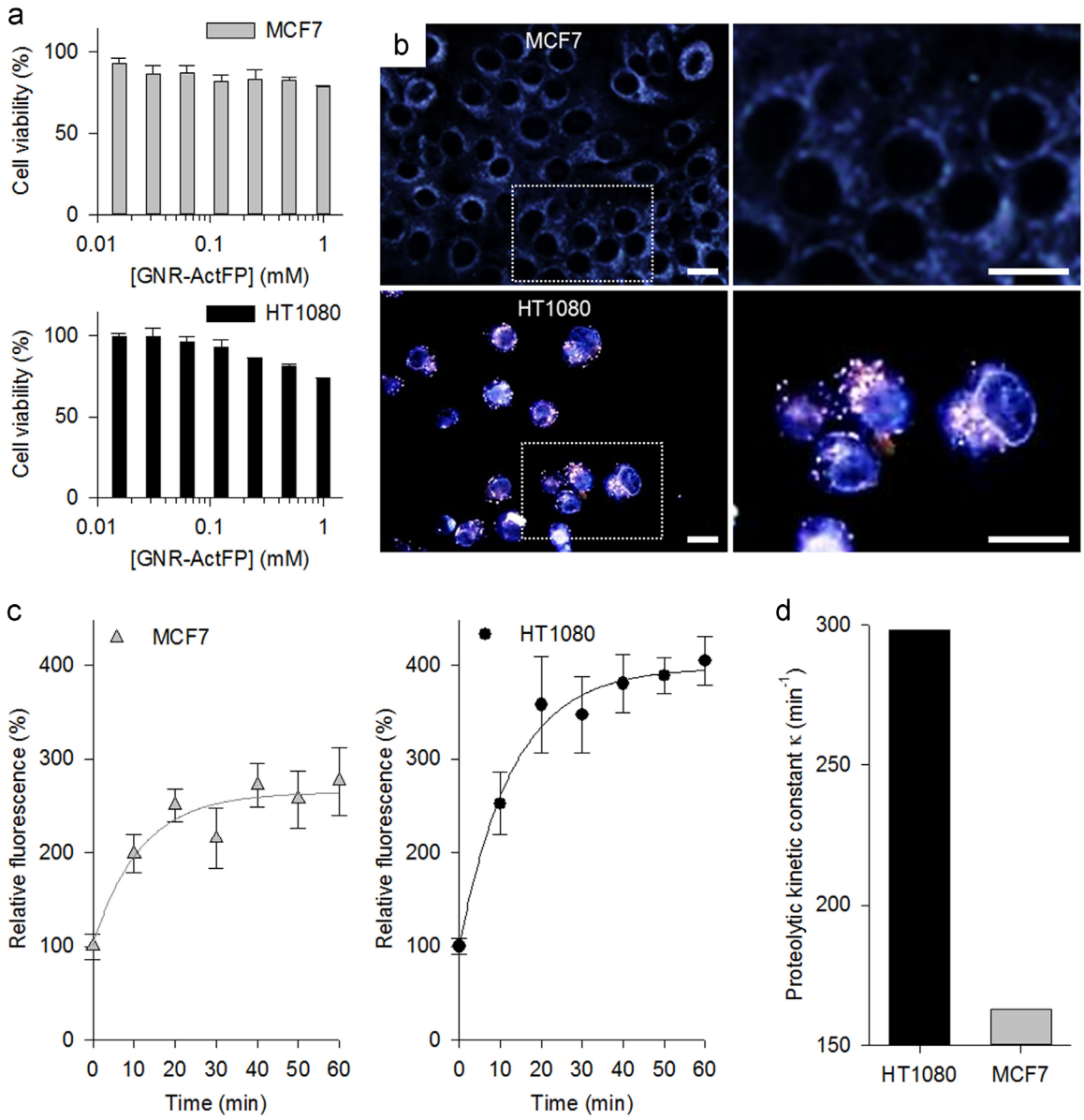

Fig. 3. Effect of GNR-ActFP on cultured cancer cells. (a) Cell viability of MCF7 (gray) and HT1080 (black) cells as a function of GNR-ActFP concentration. The data shown represent the mean ± SD (n=4). (b) Light scattering microscopic images of MCF7 (upper) and HT1080 (lower) cells treated with GNR-ActFP. The enlarged individual light scattering microscopic images are inserted in lower column. Scale bars represent 10 μm. (c) Time-dependent relative fluorescence intensity of MCF7 (gray) and HT1080 (black) cells treated with GNR-ActFP. (d) Proteolytic kinetic constant (κ) of the MT1-MMP in HT1080 and MCF7 cells calculated from (c).

present significant cytotoxic effect even at 2.00 μM, which was the concentration of GNR-ActFP applied in both *in vitro* and *in vivo* sensing studies. To assess the uptake efficiency of GNR-ActFP into target cancer cells, subsequently, dark field microscopic imaging analysis was conducted. Under white-light irradiation, non-treated HT1080 cells exhibited faint blue light, while GNR-ActFP-treated HT1080 cells emitted a bright reddish yellow light due to the scattering of GNR in the cytosol (Fig. 3b). Here, the light scattering was induced by the electrostatic interaction between GNRs and the incidence light that was selectively intense in cytoplasmic region. When incidence light passes through a relatively dense intracellular parts, the phase of the scattering light wave can be slightly changed according to the molecular reflective index. However, the intracellular GNR further enhanced the amplitude of scattering light wave of particular wavelength, while intrinsic organic molecules from non-treated cells were hard to strongly change amplitude of scattering light wave. From these results, we conclude that GNR-ActFP contain the targeting capability to MT1-MMP-anchored cancer cells.

To investigate *in vitro* proteolytic capability of GNR-ActFP, the fluorogenic potentials were analyzed for HT1080 and MCF7 cells after the treatment of GNR-ActFP (Fig. 3c and d). GNR-ActFP was excited at 746 nm for the elimination of meaningless background fluorescence from living organs (Gibbs 2012; Pansare et al. 2012). The fluorescence intensity was measured as a function of incubation time. HT1080 cells treated with GNR-ActFP presented a distinct increase in the relative fluorescence intensity, which was almost two times higher compared to MCF7 cells treated with GNR-ActFP. These results indicate that GNR-ActFP can specifically exhibit the fluorogenic activity for MT1-MMP-expressing cancer cells cultured *in vitro*.

3.4. Application of GNR-ActFP as NIR fluorogenic nanosensor in vivo

To explore the potential of GNR-ActFP as an *in vivo* fluorogenic nanosensor, furthermore, we evaluated the targeted fluorogenic

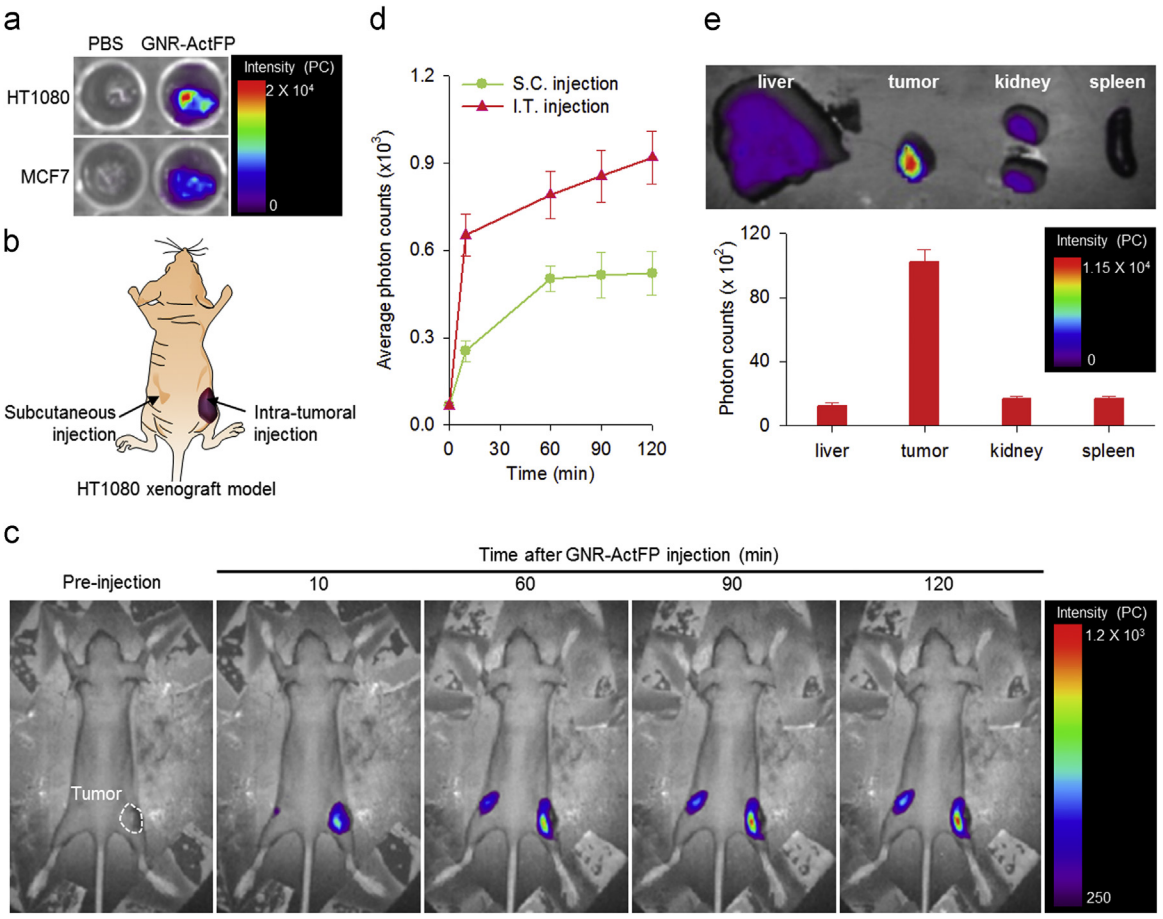

Fig. 4. Assessment of NIR fluorescence intensity from GNR-ActFP as a nanosensor *in vitro* and *in vivo* mouse xenograft tumor model. (a) *In vitro* optical fluorescence images of HT1080 and MCF7 cells after treatment of GNR-ActFP. (b) Schematic images for evaluation of GNR-ActFP targeting ability in HT1080-xenograft model. (c) *In vivo* optical fluorescence images of HT1080 tumor-bearing mice after the subcutaneous injection in normal region (left) and intra-tumoral injection in HT1080 tumor region (right) of GNR-ActFP at various time intervals, respectively. A white dashed boundary indicated tumor site. (d) Average photon counts measured from corresponding *in vivo* time-dependent NIR images of tumor region after the intravenous injection of GNR-ActFP. (e) *Ex vivo* optical fluorescence images and their quantification of the excised organs (liver, kidney and spleen) and tumor at 120 min post-injection of GNR-ActFP as recorded as total photon counts.

capability of GNR-ActFP in MT1-MMP-expressed tumor-bearing xenograft mice model. At first, we evaluated NIR fluorescence sensing potential for the prepared fluorogenic nanoprobe after the treatment with MT1-MMP-expressing or -deficient cancer cells (Fig. 4a). 2 h after the incubation of MT1-MMP-expressing HT1080 cells or MT1-MMP-deficient MCF7 cells treated with GNR-ActFP, a significant increase in cellular NIR fluorescence signal intensity from Cy7 was detected in HT1080 cells. Subsequently, GNR-ActFPs were administered to xenograft mice *via* directly intra-tumoral injection. NIR fluorescence images were monitored with an *in vivo* optical sensing system at selected time points after the injection of GNR-ActFPs as represented in Fig. 4b. After simultaneous injection of GNR-ActFP at normal left and tumoral right proximal thighs, strong NIR fluorescence signal was evidently observed at tumoral site and the fluorescence signal gradually increased over 120 min at the tumor site (Fig. 4c). 10 min after the injection of GNR-ActFP, the tumor site started to emit NIR fluorescent light and the signals from tumor were further increased over time due to the proteolytic activity by MT1-MMP. In contrast, the normal site exhibited no remarkably enhanced NIR fluorescence signals after the injection of GNR-ActFP. The total photon counts in the tumor region at 120 min after the injection of GNR-ActFP were about 43% higher compared to normal region (Fig. 4d). By considering these results, our *in vivo* fluorogenic nanosensor was effective for the characterization of MT1-MMP-expressing tumors due to their specific binding and fluorogenic potentials induced by MT1-MMP. In addition, *ex vivo* NIR fluorescence sensing for exercised organs demonstrated that the tumor tissue only exhibited strong NIR fluorescence signals (Fig. 4e). The tumor tissue exhibited 8.5-, 6.18-, and 6.18-fold higher photon counts compared to liver, kidney, and spleen, respectively (Fig. 4e). These *in vivo* fluorogenic sensing results provide strong empirical evidence for the utility of GNR-ActFP as an *in vivo* molecular sensing agent for MT1-MMP-expressing tumors.

4. Conclusions

In summary, we have formulated GNR-ActFP as a fluorogenic nanosensor and evaluated its cancer biomarker-specific targeting ability and utility *in vitro* and *in vivo*. GNR-ActFP nanosensor has developed in this study has allowed us to achieve NIR fluorogenic sensing in an optimal tissue-penetrating optical NIR window with sensitive and efficient detection of MT1-MMP activity. Our results indicate that GNR-ActFP presents a promise as NIR enzyme-activity tracker for monitoring metastatic cancer *in vivo*.

Acknowledgments

This work was supported by a National Research Foundation of Korea (NRF) grant, funded by the Korean government, Ministry of

Education and Science Technology (MEST) (2012R1A1A2006248 and 2014R1A1A2059806) and a grant from the National RD Program for Cancer Control, Ministry of Health and Welfare, Republic of Korea (1220100).

References

Andersson, A., Danielsson, J., Gräslund, A., Mäler, L., 2007. Eur. Biophys. J. 36, 621–635.
Austin, C.D., Wen, X., Gazzard, L., Nelson, C., Scheller, R.H., Scales, S.J., 2005. Proc. Natl. Acad. Sci. U. S. A. 102, 17987–17992.
Ballou, B., Fisher, G.W., Deng, J.S., Hakala, T.R., Srivastava, M., Farkas, D.L., 1998. Cancer Detect. Prev. 22, 251–257.
Bonoiu, A.C., Bergey, E.J., Ding, H., Hu, R., Kumar, R., Yong, K.-T., Prasad, P.N., Mahajan, S., Picchione, K.E., Bhattacharjee, A., Ignatowski, T.A., 2011. Nanomedicine 6, 617–630.
Cheng, Z., Levi, J., Xiong, Z., Gheysens, O., Keren, S., Chen, X., Gambhir, S.S., 2006. Bioconjug. Chem. 17, 662–669.
Choi, J., Yang, J., Bang, D., Park, J., Suh, J.-S., Huh, Y.-M., Haam, S., 2012. Small 8, 746–753.
Choi, J., Yang, J., Park, J., Kim, E., Suh, J.-S., Huh, Y.-M., Haam, S., 2011. Adv. Funct. Mater. 21, 1082–1088.
Ghosh, D., Chattopadyay, N., 2013. Opt. Photonics J. 3, 18–26.
Gialeli, C., Theocharis, A.D., Karamanos, N.K., 2011. The FEBS J. 278, 16–27.
Gibbs, S.L., 2012. Quant. Imaging Med. Surg. 2, 177–187.
Hong, Y., Ku, M., Heo, D., Hwang, S., Lee, E., Park, J., Choi, J., Jung Lee, H., Seo, M., Jig Lee, E., In Yook, J., Haam, S., Huh, Y.-M., Sung Yoon, D., Suh, J.-S., Yang, J., 2014. Biosens. Bioelectron. 57, 171–178.
Hong, Y., Ku, M., Lee, E., Suh, J.-S., Huh, Y.-M., Yoon, D.S., Yang, J., 2013. BIOMEDO 19, 051202.
Ke, S., Wen, X., Gurfinkel, M., Charnsangavej, C., Wallace, S., Sevick-Muraca, E.M., Li, C., 2003. Cancer Res. 63, 7870–7875.
Kessenbrock, K., Plaks, V., Werb, Z., 2010. Cell 141, 52–67.
Law, W.-C., Yong, K.-T., Baev, A., Hu, R., Prasad, P.N., 2009. Opt. Express 17, 19041–19046.
Lee, G., Eom, K., Park, J., Yang, J., Haam, S., Huh, Y.-M., Ryu, J.K., Kim, N.H., Yook, J.I., Lee, S.W., Yoon, D.S., Kwon, T., 2012. Angew. Chem. Int. Ed. 51, 5837–5841.
Masood, R., Roy, I., Zu, S., Hochstim, C., Yong, K.-T., Law, W.-C., Ding, H., Sinha, U.K., Prasad, P.N., 2012. Integr. Biol. 4, 132–141.
Pansare, V., Hejazi, S., Faenza, W., Prud'homme, R.K., 2012. Chem. Mater.: Publ. Am. Chem. Soc. 24, 812–827.
Park, J., Yang, J., Lim, E.-K., Kim, E., Choi, J., Ryu, J.K., Kim, N.H., Suh, J.-S., Yook, J.I., Huh, Y.-M., Haam, S., 2012. Angew. Chem. Int. Ed. 51, 945–948.
Peng, C.-A., Pachpinde, S., 2014. Nanomater. Nanotechnol. 4, 9.
Quek, C.-H., Leong, K.W., 2012. Nanomaterials 2, 92–112.
Seiki, M., 2003. Cancer Lett. 194, 1–11.
Si, S., Leduc, C., Delville, M.-H., Lounis, B., 2012. ChemPhysChem 13, 193–202.
Smith, L., Kuncic, Z., Ostrikov, K., Kumar, S., 2012. J. Nanomater. 2012, 7.
Tiwari, P., Vig, K., Dennis, V., Singh, S., 2011. Nanomaterials 1, 31–63.
Tsai, C.-L., Chen, J.-C., Wang, W.-J., 2001. J. Med. Biol. Eng. 21, 7–14.
Xiao, Y., Jaskula-Sztul, R., Javadi, A., Xu, W., Eide, J., Dammalapati, A., Kunnimalaiyaan, M., Chen, H., Gong, S., 2012. Nanoscale 4, 7185–7193.
Zhai, Y., Hotary, K.B., Nan, B., Bosch, F.X., Muñoz, N., Weiss, S.J., Cho, K.R., 2005. Cancer Res. 65, 6543–6550.
Zhang, Z., Wang, J., Chen, C., 2013. Theranostics 3, 223–238.
Zou, P., Xu, S., Povoski, S.P., Wang, A., Johnson, M.A., Martin, E.W., Subramaniam, V., Xu, R., Sun, D., 2009. Mol. Pharm. 6, 428–440.